Journal of Marine Research, 77, 267–296, 2019

Recirculating flow in a basin with closed f/h contours

by Alexander M. Fuller[1,2], Thomas W. N. Haine[1] and Erik Kvaleberg[3]

ABSTRACT

A general circulation model is used to study the time evolution of a rotating, weakly baroclinic fluid in a basin with sloping sidewalls. Contours of f/h, where f is the Coriolis parameter and h is the depth of the fluid, are closed in this model. The fluid is forced by a localized source of positive vorticity. The initial response is a narrow, recirculating cell that resembles a β-plume modified by bathymetry. Such cells have been found in previous studies and have been linked to the recirculation cells observed in the subpolar North Atlantic. However, this is not a steady solution in this basin with closed f/h contours, and the circulation evolves into a gyre that encircles the basin. The time at which this transition occurs depends on the Rossby number, with higher Rossby numbers transitioning earlier. Based on the budget of potential vorticity, an argument is made that the western boundary is not long enough to drain significant vorticity from the flow and therefore a bathymetric β-plume is not a steady solution. A similar argument suggests that the Labrador Sea cannot sustain steady, linear, barotropic recirculations either. We speculate that the observed recirculations depend on inertial separation at sharp bathymetric gradients to break the assumption of linearity, which leads to significant viscous dissipation.

Keywords: beta-plume, recirculation, Labrador Sea, vorticity dynamics, multiple equilibria

1. Introduction

The main feature of the circulation in the Irminger and Labrador Seas is a swift geostrophic current flowing around the coast of Greenland, across Davis Strait, and south along Labrador. During its course, its name changes from the Irminger Current/East Greenland Current to the West Greenland Current, and finally to the Labrador Current, but in the following it is referred to simply as the *boundary current*. Figure 1a shows a schematic of this circulation. It is a familiar feature of the subpolar ocean (Sverdrup et al. 1942; Schmitz and McCartney 1993), but until the advent of satellite measurements, little was known about the details of the interior Labrador Sea circulation. Sea surface temperature and sea surface height (SSH) measurements revealed an energetic interior with an area of eddy formation off the West Greenland shelf (Lilly et al. 2003).

1. Department of Earth and Planetary Sciences, Johns Hopkins University, Baltimore, MD 21218, USA.
2. Corresponding author: ***e-mail: alex.fuller1@gmail.com***
3. Norwegian Armed Forces, Oslo, Norway.

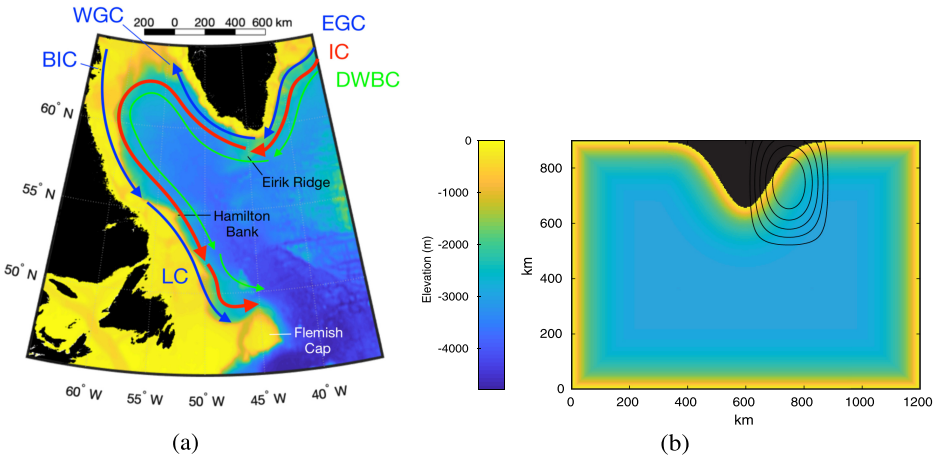

Figure 1. (a) Circulation of the Labrador Sea, showing the East Greenland Current (EGC), Irminger Current (IC), Deep Western Boundary Current (DWBC), West Greenland Current (WGC), Baffin Island Current (BIC), and Labrador Current (LC). (b) Idealized model domain used in this paper. The black contours show the positive wind stress curl, which is highest in the center. The color scale applies to the bathymetry of both figures.

Profiling Lagrangian floats were deployed in the Irminger and Labrador Seas in the late 1990s and mapped out several sub basin-scale recirculations (Lavender et al. 2000, 2005). These recirculations are present in the hydrographic data of Hall et al. (2013) as alternating bands of velocity near the Greenland coast, indicating the different sides of a coastal recirculating gyre. Holliday et al. (2009) found that observations agreed with the scheme of Lavender et al. (2005), with recirculating cells on either side of Eirik Ridge and net flow from the Labrador Sea into the Irminger Sea, although they found that the boundary current is not continuous across the ridge. Some recirculations add to it and some subtract from it.

Others have combined the float data with general circulation models to estimate the circulation. Faure and Speer (2005) used data assimilation to calculate a stream function for the subpolar North Atlantic at 1,500 m depth. They constrained averaged float data with the conservation of barotropic potential vorticity (PV; see Faure and Speer 2005, fig. 6a). Because the circulation is linear, forced, undamped, and barotropic, f/h is conserved, where f is the Coriolis parameter and h is the depth of the water. The streamlines are concentrated near the continental shelves and seem to follow the bathymetry. This suggests a mid-depth boundary current that flows unbroken from the Irminger Sea to the Labrador Sea and around to Grand Banks. Recirculations appear east of Greenland in the Irminger Sea and in the interior Labrador Sea.

Forget et al. (2008) estimated the circulation by assimilating data from Argo floats. They found that the mid-depth velocities agreed with the drift maps of Lavender et al. (2000).

Both showed velocities in excess of 5 cm s^{-1} along the coasts of Greenland and Canada, but not in the rest of the subpolar gyre, and cyclonic recirculations in the Labrador Sea. The circulation estimated from Argo data lacked a closed recirculation in the Irminger Sea, however.

Estimates of the circulation show a narrow, recirculating cell in the western part of the Irminger Sea (Holliday et al. 2007; Våge et al. 2011), whereas others exist in the Labrador Sea. Because they are inferred from data averaged over timescales longer than those of transient eddies, they are a permanent feature of the circulation. They are cyclonic, situated offshore close to the shelf break, and have velocities of about 5 cm s^{-1}. Their cross-shelf extent is 200–300 km, whereas their along-shelf extent is longer, giving the cells a stretched appearance. Similar recirculations appear in the high-resolution simulations of Käse et al. (2001).

The dynamical origin of these recirculating cells was addressed by Spall and Pickart (2003) (hereafter SP03). They used an idealized numerical model of the subpolar North Atlantic with a rectangular basin and a peninsula extending south from the northern boundary (representing Greenland) that partially separated the model into Labrador and Irminger Seas. Their results showed that when a cyclonic, seasonal wind stress was applied east of the peninsula, the resulting time-averaged circulation resembled the float data of Lavender et al. (2000, 2005). Water flows westward, around the coast of Greenland, and southward along the western boundary. The vorticity that is added to the flow by the wind is lost in a viscous western boundary layer in order to balance the overall vorticity budget. Once the vorticity has been dissipated into the boundary layer, the flow retroflects and returns to the forcing region, creating a recirculating cell. The region of minimum SSH in this cell is located off the Greenland coast. SP03 referred to these dynamics as a time-dependent, stratified, bathymetric β-plume. For the original formulation of a β-plume, see Stommel (1982). The β-plume is a Green's function for the Stommel model of ocean circulation, namely, a homogeneous fluid over a flat seafloor, with linear drag, negligible inertia, and a point source of vorticity forcing (Vallis 2006). Its streamlines are distributed as if they advected westward and diffused like a passive tracer. In an ocean with uniform depth, the rate of advection is governed by $\beta = df/dy$, the gradient of planetary vorticity, hence the name β-plume.

SP03 concluded that a seasonally varying wind stress east of Greenland is sufficient to explain the recirculating cells in the oceanographic data. Their model, however, had sloping northern and western walls, but vertical southern and eastern walls. Contours of f/h therefore terminate in the southwest corner. The fluid cannot navigate this corner and conserve PV and instead retroflects, returning to the forcing region and forming a closed recirculation. In this study, we show that when f/h contours do not terminate there but continue around the basin, another type of circulation exists (a basin-wide gyre) and seems to be the only stable solution.

Haine and Fuller (2016) (hereafter HF16) established the theory of the budget of PV for β-plumes, including in the presence of a boundary. Their model was a semi-infinite ocean

with a flat seafloor and a straight coastline bounding the ocean in one direction. This was a first step in explaining the existence of recirculations in the subpolar North Atlantic, but that model is not representative of the real ocean. In this paper we take another step by using an idealized model similar to that of SP03 and calculating the budget of PV along the western boundary. We then do the same using the bathymetry of the Labrador Sea. We find that within a realistic domain, localized recirculations driven by strong forcing exist only as quasi-steady states because, in the presence of varying bathymetry, viscous dissipation is not strong enough to produce the required closure.

Dynamical results from two limiting cases are useful for context: First, PV conservation for unstratified (barotropic) flow, without forcing or dissipation, requires that streamlines coincide with $\frac{f}{h} + \frac{1}{h}\nabla \cdot \left(\frac{1}{h}\nabla\psi\right)$, where ψ is the stream function (HF16). There is no depth dependence in the circulation. If the flow is also linear (relative vorticity is negligible), then streamlines coincide with f/h contours. Flow perpendicular to f/h contours is a local response proportional to the local forcing; flow parallel to f/h contours is a nonlocal response, determined by integrating along the f/h contours (Koblinsky 1990). Second, stratified (baroclinic) flow diminishes the effects of bathymetry. Under some circumstances, the stratification can isolate the circulation to shallow depths so that the bottom fluid is resting. In this way, the upper circulation can be shielded from the effects of bathymetry and PV conserving flow follows contours of planetary vorticity f as in subtropical gyre theory. This reduction of the importance of bathymetry by stratification is called baroclinic compensation (Bogden et al. 1993; Marshall 1995; Marshall and Stephens 2001). In general, one expects baroclinic compensation to be incomplete, in which case the stratified circulation is influenced by both f and h contours.

Some caveats for the physical oceanographer: this paper is about wind-forced circulation in a weakly stratified ocean. As such it neglects convection and three-dimensional overturning. The familiar water masses of the subpolar North Atlantic, like Denmark Strait Overflow Water, Labrador Sea Water (LSW), and North Atlantic Deep Water, are not considered here. For a review of these topics, the reader is referred to Deshayes et al. (2007), Haine et al. (2008), or Palter et al. (2008). Also absent is a northward flowing western boundary current, like the Gulf Stream. Spall (1996) showed that intense mixing occurs at the crossover of the Gulf Stream and the Deep Western Boundary Current (DWBC) near Cape Hatteras. Eddy fluxes of PV entrain the upper DWBC into the interior, where it recirculates with the gyres. With no Gulf Stream, as in this study, this mixing and entrainment do not feature. Finally, although a region of intense wind stress curl off the east coast of Greenland is realistic (Daniault et al. 2011), no heat flux is allowed, which is an important feature of the real Greenland tip jet (Pickart et al. 2003). Only the wind's mechanical effect is modeled, not its thermal effect.

We describe the numerical model in section 2 and our results in section 3. In section 4 we connect the results to the work of HF16. The discussion and conclusions are given in section 5.

2. Model configuration

Numerical experiments are performed with the Massachusetts Institute of Technology general circulation model (MITgcm; Marshall et al. 1997). The model domain is shown in Figure 1b. It is a rectangular basin 1,200 × 900 km. The horizontal grid resolution is 7.5 × 7.5 km. Depth $h(x, y)$ is measured positive upwards from the resting sea surface in the z direction and has a deepest value $H = -3{,}000$ m. Greenland is idealized as a Gaussian curve on the northern side of the domain. All sidewalls slope down exponentially with an e-folding length $l = 60$ km. For comparison, SP03 used vertical sidewalls except at the northern and western walls, where $l = 60$ km.

We use two vertical discretizations, one with eight geopotential levels equally spaced 375 m apart, and one with two levels 1,500 m apart. The model has a Cartesian $x-y$ coordinate system and is forced by a zonal wind stress of the form

$$\tau^x(x, y) = \tau_0 \sin\left(\frac{2\pi x}{\lambda_x}\right)\left[1 - \cos\left(\frac{2\pi y}{\lambda_y}\right)\right] \tag{1}$$

over the rectangular region $600 < x < 900$ km, $495 < y < 900$ km, with $\lambda_x = 600$ km and $\lambda_y = 1{,}004$ km. The resulting wind stress curl is

$$\hat{\mathbf{k}} \cdot \nabla \times \vec{\boldsymbol{\tau}} = -\frac{2\pi\tau_0}{\lambda_y} \sin\left(\frac{2\pi x}{\lambda_x}\right) \sin\left(\frac{2\pi y}{\lambda_y}\right), \tag{2}$$

where the characteristic strength of the wind stress τ_0 is negative to give a positive (cyclonic) curl. The black contours in Figure 1b illustrate the curl. Its peak magnitude is 1.56×10^{-6} Nm^{-3}, very similar to that used by SP03. This is 30% stronger than the climatological winter wind stress curl (Renfrew et al. 2002) and many times stronger than the annual average wind stress curl (Mesinger et al. 2006; Våge et al. 2011). Therefore it should not be considered representative of the long-term forcing in the Irminger Sea. Our aim is to be consistent with SP03 and to explore geophysical fluid dynamics.

The model is hydrostatic and run on a β-plane with $f = f_0 + \beta y$, where $f_0 = 1.2 \times 10^{-4}$ s^{-1}. The horizontal Laplacian diffusivity of heat is 20 $\mathrm{m}^2\mathrm{s}^{-1}$ and that of momentum $\nu = 50$ $\mathrm{m}^2\mathrm{s}^{-1}$. In the vertical direction they are both 10^{-5} $\mathrm{m}^2\mathrm{s}^{-1}$. The horizontal momentum coefficient is probably an order of magnitude smaller than in the Labrador Sea (Funk et al. 2009), but is used for consistency with SP03. As shown in section 4, an increase of one or even two orders of magnitude does not qualitatively change the results.

The Munk length (Munk 1950) can be estimated from

$$\delta_M = \left(\frac{\nu}{\beta}\right)^{1/3}. \tag{3}$$

Taking β at 60°N, the latitude of Cape Farewell, gives $\delta_M = 16$ km. However, over the sloping sidewall of the western boundary in Figure 1b, topographic β dominates planetary β. Using instead effective β gives $\delta_M = 5$–9 km over the main part of the slope. This is the

e-folding length of changes in the current speed, so we expect the full width of a viscous current to span several multiples of δ_M. Thus a 7.5-km grid should suffice.

The inertial length can be estimated from

$$\delta_I = \left(\frac{U}{\beta}\right)^{1/2} \tag{4}$$

by taking a characteristic horizontal speed $U = 5$ cm s^{-1}. Planetary β gives 66 km and effective β 15–25 km. This estimates the width of the western boundary current. The boundary conditions are no-slip along the walls and free-slip along the bottom. Because $\delta_I/\delta_M \approx$ 2–4 (depending on β), there is a viscous sublayer along the coastline to satisfy the no-slip condition (Pedlosky 1996).

Finally, we can compare the model resolution to the deformation radius, because resolving this scale is important for long baroclinic wave speed. In a continuously stratified fluid, the deformation radius $L_d = Nh/f$, where N is the buoyancy frequency, given by

$$N^2(z) = -\frac{g}{\rho}\frac{\partial \rho}{\partial z} \approx -\frac{g}{\rho_0}\frac{\Delta \rho}{\Delta z}. \tag{5}$$

ρ is the density of the fluid, ρ_0 is the average density (assumed to be much larger than the variations), and g is gravitational acceleration, 9.81 ms^{-2}. The model starts with temperature stratification $\Delta T = 1$°C (5°C in the top level, 4°C in bottom). The equation of state is linear with a thermal expansion coefficient $\alpha_T = 2 \times 10^{-4}$ °C^{-1} and salinity is uniform. Therefore density is proportional to temperature, $\Delta \rho = -\rho_0 \alpha_T \Delta T$, and Eq. (5) becomes

$$N^2 = \frac{g \alpha_T \Delta T}{H}. \tag{6}$$

Then we have

$$L_d = \frac{\sqrt{g H \alpha_T \Delta T}}{f}, \tag{7}$$

which, with the values given above, is 20 km. This suggests that the model has two to three grid points per deformation radius. Measurements indicate that eddies in the Labrador Sea are about 10 km across (Funk et al. 2009), so this model is potentially eddy-permitting, although we do not see any eddies in the simulations, presumably because the flow is stabilized by the bottom slope.

In the next section, β, τ_0, and ν are varied systematically and the corresponding circulations are cataloged. Each of these variables affects the model in a different way, and we wish to know how they alter the long-term circulation.

3. Numerical results

The numerical solutions are best understood by looking first at a snapshot of a model that exhibits the expected linear response. We expect the early circulation to resemble a linear

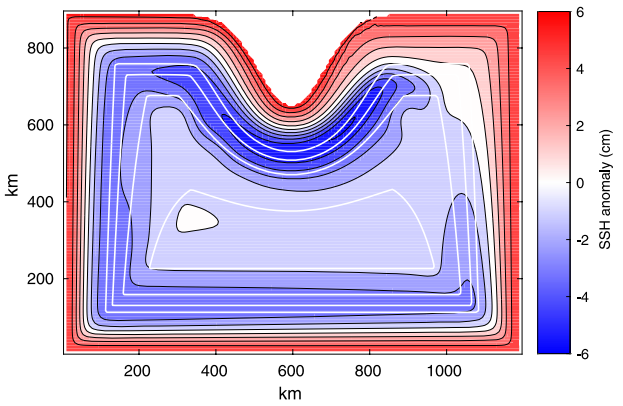

Figure 2. SSH anomaly (cm) after 10 years of forcing with $\beta = 1.22 \times 10^{-11}$ m^{-1}s^{-1}. f/h contours are shown in white.

β-plume that follows the bathymetry in the direction of dynamical west. Dynamical west was introduced in HF16 for the steady, linear, barotropic vorticity equation and describes how the preferred westward distribution of streamlines is modified due to bathymetry and friction. It will be explored more in section 4. We then look at the time evolution of a model at a given value of β, followed by the long-term, steady-state solutions of many models at different values of β. This shows that the dynamics of even this simple model are complex.

a. The β-plume

Figure 2 shows a typical β-plume solution after 10 years of integration. The SSH anomaly is shown in red and blue, and f/h contours are shown as white lines. In this case $\beta = 1.22 \times 10^{-11}$ m^{-1}s^{-1} and $\nu = 50$ m^{2}s^{-1}. The SSH has a minimum just southwest of the forcing region at $x = 700$ km, $y = 600$ km. A long, narrow region of low SSH wraps around the peninsula and continues south along the western boundary. This is similar to the β-plume found in SP03 and the recirculating cells in the data. Here, several SSH contours reach partway up the eastern boundary before retroflecting. Because h varies much more rapidly than f near the coast, f/h contours are very nearly h contours. Only near the center of the domain, where the bottom slope is very weak, do f and h have comparable gradients. The recirculating cell therefore seems to follow bathymetry.

The flow in Figure 2 has $U \approx 5$ cm s^{-1} or less. Using $f = 1.2 \times 10^{-4}$ s^{-1} and $L =$ 1,000 km, the Rossby number $Ro = U/fL$ is order 10^{-4}, so the circulation outside of the forcing region is geostrophic. Furthermore the magnitude of relative vorticity U/L is much less than βL for $\beta = 1.3 \times 10^{-11}$ m^{-1}s^{-1}, so the flow is also linear. SSH and f/h contours do not coincide exactly because the flow is baroclinic and not steady. The model is still evolving after 10 years. In particular, SSH contours continue to move counterclockwise

around the perimeter of the basin. We examine the time evolution of the model below, but first we address the dynamics at work in Figure 2.

The explanation for this circulation is that of a stratified, bathymetric β-plume. The β-plume was first described by Stommel (1982) and is most readily demonstrated by the inviscid linear vorticity equation,

$$\beta v = f \frac{\partial w}{\partial z}, \tag{8}$$

where v is meridional velocity and $\partial w/\partial z$ is the change in vertical velocity with height. In the northern hemisphere, inside a forcing region where $\partial w/\partial z$ is positive (cyclonic wind stress), Eq. (8) predicts a northward transport (Pedlosky 1987). Outside this region, however, $\partial w/\partial z = 0$, and there can be no inviscid meridional transport. In an open ocean with flat bathymetry, water must leave from and return to the forcing region as a zonal current. At some point west of the forcing region, the circulation is closed by viscous effects, perhaps at a solid wall whose dynamics are not contained in Eq. (8). Thus, in a zonal channel with isolated forcing in the east, the result is a plume with westward transport to the north and a returning eastward transport to the south.

In the β-plume in Figure 2, which has sloping bathymetry, the fluid vorticity is modified first by the input of cyclonic vorticity from the wind stress. It then wraps around the coast of Greenland and proceeds westward until it reaches the western boundary. If the forcing is strong enough, the plume continues south along the boundary, crossing lines of planetary vorticity. The vorticity change resulting from both the wind stress and the southward flow is offset in a viscous western boundary layer, and the current retroflects and returns to the forcing region to close the circulation.

b. Transition to a gyre

Sverdrup balance and Eq. (8) describe the β-plume in Figure 2, modified appropriately for the presence of bathymetry (see HF16). In the long term, however, Sverdrup balance is not appropriate inside a region of closed f/h contours (Koblinsky 1990). In these regions, time-dependent dynamics and friction can influence the barotropic flow. Even a small amount of friction can alter the global state of a recirculating fluid because it has unbounded time to act (Pedlosky 1996).

To see how this affects the circulation, we look at the time evolution beyond 10 years. Figure 3 shows snapshots of SSH anomaly of a model with $\beta = 1.20 \times 10^{-11}$ m^{-1}s^{-1} that started from rest and ran for 40 years. The first panel shows the result after 1 year. A region of closed SSH contours exists beneath the forcing region. In the linear limit, this feature is a projection of the classic β-plume onto the f/h contours of the basin (white lines in the last panel). The plume wraps around the peninsula, following lines of f/h. Other SSH contours near the perimeter wrap all the way around the basin.

For several more years, the β-plume extends farther west. SSH contours reach south along the western boundary, east along the southern boundary, and north along the eastern

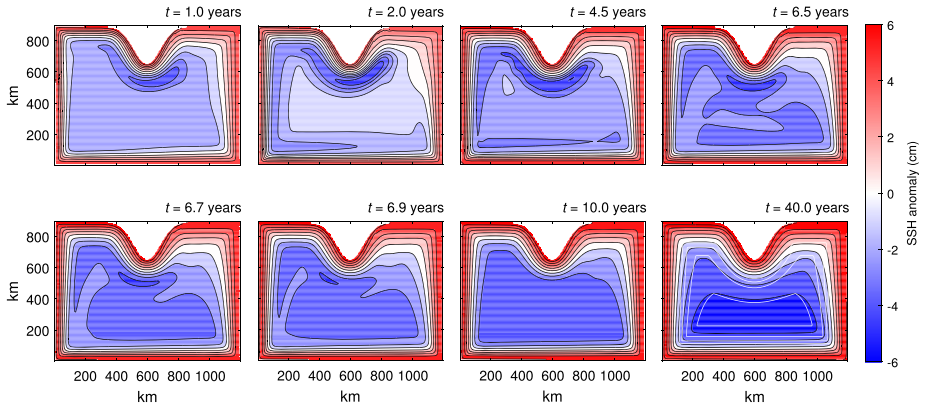

Figure 3. The time evolution of an 8-level model started from rest and run for 40 years, with $\beta = 1.20 \times 10^{-11}$ m^{-1}s^{-1}. The times were chosen to illustrate the different stages of the circulation's development. White lines in the last panel show f/h contours.

boundary. After year 5 they begin to enter the forcing region and reconnect. In the barotropic geostrophic limit, streamlines coincide with f/h contours and a fluid parcel would follow the perimeter of the domain, not recirculate. From years 6 to 7, the circulation quickly changes, with all the SSH contours spreading out to form a single cyclonic gyre around the basin. This process is complete by year 10. From years 10 to 40, the SSH in the middle of the domain deepens and aligns more closely with f/h contours, and the circulation strengthens. In this paper, we define a gyre to be similar to this final state, with SSH that generally follows f/h contours. By contrast, a β-plume crosses f/h contours.

The transition from a β-plume to a gyre is mostly complete after 10 years. The time at which this transition occurs, however, is a strong function of β. Figure 4 shows the evolution of a model with $\beta = 1.22 \times 10^{-11}$ m^{-1}s^{-1}, just 1.7% larger than in Figure 3. The β-plume now persists for decades, and the last streamline does not reconnect until year 172. The first 10 years are not long enough to reach a steady state. SP03 argued that the circulation adjusts within 10 years because baroclinic Rossby waves, with phase speed $c_\phi = \beta L_d^2$, can traverse the domain in this time. In this case, the phase speed is around 5×10^{-3} ms^{-1}, which implies a basin-crossing time L/c_ϕ of about 7.5 years. Therefore all information about the initial and boundary conditions has propagated through the domain after a decade.

This seemed to be correct: time series of transport and SSH from years 8 to 10 showed no long-term trend. But the switch from open to closed f/h contours fundamentally changes the problem. Inside a region of closed f/h contours, baroclinic pressure torque can dramatically influence the depth-averaged circulation (Koblinsky 1990). We find a slower evolution superimposed on this decadal adjustment. Indeed, further simulations at larger β suggest that this slow evolution always occurs and the transition to a gyre is only delayed. It seems that a β-plume in this model is not absolutely steady. We explore this idea further in section 4.

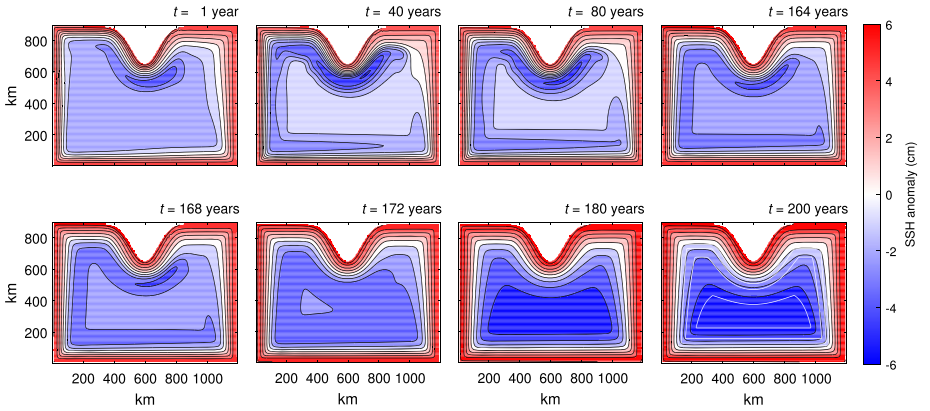

Figure 4. Similar to Figure 3, but with $\beta = 1.22 \times 10^{-11}$ m^{-1}s^{-1} and different times. The transition from β-plume to gyre occurs much later than in Figure 3, at 172 years. See also Figure 2.

Note that the transition from a β-plume to a gyre in Figures 3 and 4 is fast. In Figure 3 it occurs in less than one year, after 5–6 years in the β-plume state. In Figure 4 it occurs in 3–4 years, after 170 years in the β-plume state. The transition occurs on the timescale of years, whereas the circulation may spend decades to centuries as a β-plume before and, presumably, infinitely long as a gyre after. Note also that the transition occurs later for larger β (Figs. 3 and 4, see also Fig. 7). This sense is opposite to the increase in Rossby wave phase speed c_ϕ with β quoted above. This fact, plus the sensitive dependence on β and the very long time compared to L/c_ϕ for transition of the β-plume in Figure 4, suggests that linear Rossby wave dynamics are not controlling the final equilibration of the flow.

c. The β effect

We see from Figures 3 and 4 that the gyre circulation is stronger than the β-plume circulation. This is demonstrated by the fact that the SSH anomaly in the middle of the gyre is lower than it is in the middle of the β-plume. We can calculate the transport from the velocity fields by summing the normal component of velocity across a vertical plane between the SSH minimum and the nearest coastal point. As long as the gyre always has a stronger circulation than the β-plume, we can use transport as a metric to distinguish unique model states and plot the solutions against a parameter of choice.

The relevant measure of nonlinearity for our problem is the β-Rossby number,

$$R_\beta = \frac{\tau_0}{\rho_0 \beta^2 H L^3}, \tag{9}$$

which emerges naturally from the barotropic vorticity equation by assuming the leading order flow is in Sverdrup balance. Like the traditional Rossby number, the β-Rossby number

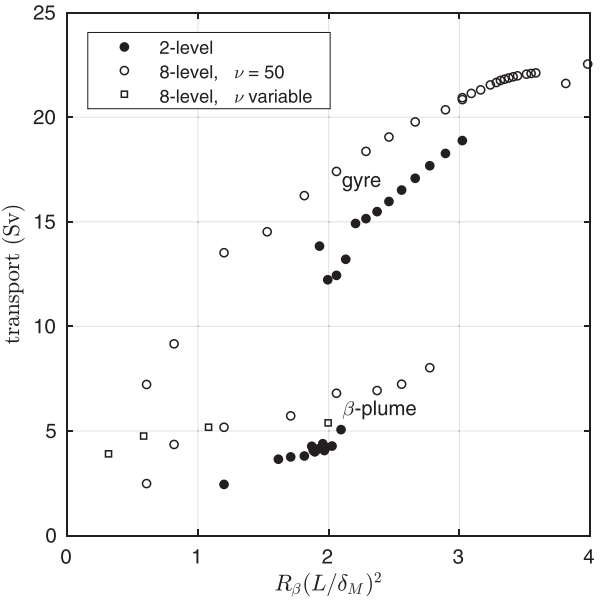

Figure 5. Transport (Sv) versus $R_\beta(L/\delta_M)^2$, the characteristic scale of the vorticity advection term in the western boundary layer. The upper branch corresponds to gyres and the lower branch to β-plumes.

is the ratio of inertial acceleration to Coriolis acceleration in a barotropic fluid, on a β-plane, and forced by wind stress τ_0 (Vallis 2006). Note, however, that R_β need not be order one for nonlinearity to be important. In the western boundary current, the vorticity advection term scales as

$$R_\beta \left(\frac{L}{\delta_M}\right)^2 \propto \frac{\tau_0}{\beta^{4/3}\nu^{2/3}}, \tag{10}$$

which can be order one even for small R_β if $L/\delta_M \gg 1$, as it is in our experiments. Dynamically, beta and viscosity play a similar role, both acting to decrease the nonlinear term, while the wind stress increases it.

We plot the model solutions in the parameter space of transport versus the vorticity advection scale in Eq. (10). Transport is a volume flux measured in Sverdrups (Sv), where 1 Sv = 10^6 m^{3}s^{-1}. Figure 5 shows the results for the 8- and 2-level simulations. The 8-level simulations with $\nu = 50$ m^{2}s^{-1} are shown as open circles and represent the state of the simulation after at least 200 years of model time. The 8-level simulations with variable ν are shown as open squares. These are much more viscous and evolve much more slowly than the other experiments. From inspection of the SSH field, we see little point in simulating the full 200 years, so these data points represent the state after only 100 years. The 2-level simulations are shown as black circles and represent the state after at least 400 years.

We see immediately that there seem to be two distinct branches of solutions: a lower branch with transport less than 7 Sv and an upper branch with transport greater than about 15 Sv. The lower branch corresponds to β-plume solutions and the upper branch corresponds to gyre solutions. In between is an empty region with no data points.

It is helpful to picture how these data points evolve in time. The models start from rest with zero transport, so the data points begin at the bottom of Figure 5. As the wind spins up the fluid, the models develop an initial β-plume and the data points move vertically upward. This process is faster at higher $R_\beta(L/\delta_M)^2$. After a certain time, some of these points jump to the top of the figure. This is the fast transition to a gyre. They then continue to move upward more and more slowly. The upper branch is evidently their final state. The empty space between the gyre and β-plume branches indicates that the branches are stable (or marginally stable), but all points in between are unstable.

As mentioned, the β-plume seems to be *nearly* steady (defined more precisely in section 3e), with some simulations spending centuries there before transitioning to a gyre. It is therefore computationally unfeasible to run every simulation forward long enough to see (or not see) a transition. The cutoff for the 8-level model, then, is 200 years. If a simulation has not transitioned by this time, it is deemed to be steady. The bottom branch of open circles in Figure 5 represents these simulations. It was obtained by starting models from rest. After 200 years they were observed to still be in the β-plume state. The upper branch of open circles was obtained in one of two ways. Some points represent the state of a simulation started from rest and run for 200 years, as before. However, this is too expensive to repeat for many values of β. Most of the upper branch, therefore, was obtained by restarting 200-year simulations with a slightly higher or lower β and running forward at least another 10 years. In this way it is feasible to map out the upper branch in 300–400 years of model time by starting at the end of a 200-year simulation and progressively stepping towards lower $R_\beta(L/\delta_M)^2$, as opposed to waiting until a solution evolves to a gyre from rest. A similar procedure was used to map out the 2-level branch.

For the 8-level case, the transport of both branches increases with the vorticity advection scale. The circulation becomes more inertial, whether from lower β, lower viscosity, or stronger wind. There is a range over which both gyre and β-plume persist for centuries. We can say with confidence that above $R_\beta(L/\delta_M)^2 \approx 2.8$, a β-plume vanishes within 200 years. Below that, we can merely say that it does not. We conjecture that it would vanish too, given enough time, because the models are still evolving after 200 years. Given the extreme sensitivity to β, however, this process may take millennia in some cases. For $R_\beta(L/\delta_M)^2 < 2.8$, both branches exist in a quasi-steady state. The β-plume solution is reached by running forward from rest or by stepping there from a nearby solution. The gyre solution is reached only by stepping there from a solution at higher $R_\beta(L/\delta_M)^2$.

The 2-level runs are computationally much cheaper than the 8-level runs, and so the cutoff is 400 years for them. The model state at that time is considered the long-term steady state. We see in Figure 5 that a branch of β-plume solutions exists below $R_\beta(L/\delta_M)^2 = 2.1$. Above this value, only a gyre branch exists and the transport increases linearly (with a

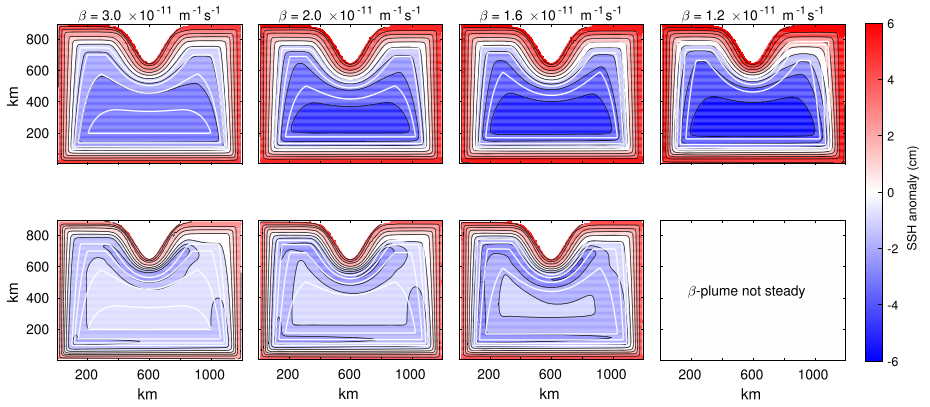

Figure 6. Sea surface height (SSH) anomaly (cm) for 8-level simulations with different values of β. The rows illustrate the two different types of circulation: gyre (upper row) and β-plume (lower row). The white lines show the same f/h contours. In the last column, only the gyre solution is steady in the long term; the β-plume disappears within a few years (see Fig. 3).

positive offset). In every simulation above 2.1, the circulation transitioned to a gyre within 400 years. This supports the hypothesis that the 8-level simulations would also eventually transition to a gyre.

Near $R_\beta(L/\delta_M)^2 = 1.9$, the long-term solution seems to change. Two-level simulations below this threshold maintain a β-plume despite their provenance in a branch of gyre solutions. The circulation of these simulations, which began as a β-plume and evolved into a gyre, has evolved *back* into a β-plume. For even smaller values of $R_\beta(L/\delta_M)^2$, the β-plume persists. This is the only part of parameter space where a β-plume seems to exist indefinitely, although we show that this is likely untrue: the circulation still creeps towards a gyre state, but very slowly.

Figure 6 shows the SSH anomaly from several 8-level simulations in Figure 5. The upper row shows the gyre circulation and the lower row shows the β-plume, for the same values of β. The solutions in each column were attained for the given value of β. All simulations were run for at least 200 years to ensure steady- or nearly steady-state conditions. The white lines show the same f/h contours, which change position from column to column with changing β. β decreases (R_β increases) from left to right. This illustrates the regime in Figure 5 where both types of circulation seem to be steady solutions.

As β decreases, the β-plume increases in length, as measured by the darker blue contours that encircle the basin, but it is restricted by the size of the domain. When $\beta = 3.0 \times 10^{-11}$ m^{-1}s^{-1} the boundary current flows counterclockwise along the northern, western, and southern boundaries, and moves partway up the eastern wall before retroflecting and returning to the forcing region. When $\beta = 1.6 \times 10^{-11}$ m^{-1}s^{-1}, the boundary current reaches around the basin and returns to the forcing region from the east. For β =

1.2×10^{-11} $m^{-1}s^{-1}$, the β-plume disappears within a few years (Figure 3) and we see a cyclonic, basin-wide gyre that follows f/h contours, with a region of low SSH in the interior. This gyre does not occur when the southern boundary is a vertical wall (SP03). The solution structure depends qualitatively on the continuity of the f/h contours. When they terminate at a vertical wall, the flow is unable to navigate the corner and remain steady and linear. Other terms must become important. But when f/h contours encircle the domain, the flow can continue eastward on its trajectory.

Consider that the inertial scale δ_I increases as β decreases (Eq. 4). With $\beta = 2.0 \times 10^{-11}$ $m^{-1}s^{-1}$, the inertial boundary layer is 50 km wide; with $\beta = 1.2 \times 10^{-11}$ $m^{-1}s^{-1}$, it increases to 65 km. Physically, the associated western intensification controls the width of the boundary current, and larger β produces a narrower flow. Conversely, the boundary current widens with decreasing β. Frictional interactions between the current and the side walls are stronger with a narrow flow, hence a narrow current (larger β) is able to shed vorticity faster than a broad flow and retroflect earlier, as seen. This idea is developed further in section 4.

d. Forcing and dissipation

We now consider how these results change when the characteristic wind stress τ_0 and the horizontal momentum diffusivity ν change. Table 1 gives a partial list of the 8-level numerical experiments.

Model times with an asterisk denote experiments that were started at the end of another experiment. Experiment 10, for example, ran from years 350 to 360 as part of a daisy-chained simulation with progressively larger β. The criterion for the existence of a β-plume is the presence of a well-developed trough wrapping around the Greenland peninsula, as seen in Figure 2. Note that in several cases, both types of circulation exist for the same set of parameters, for example, experiments 11 and 12.

Experiments 1–14 vary β and are described above. Experiments 15–19 vary ν logarithmically from 50 to 2,000 m^2s^{-1}. As ν increases, the final transport at the end of 100 years decreases, and all experiments are still in the β-plume state. These data points are shown in Figure 5 as open squares. They are not stationary: they are slowly evolving toward higher transport at 100 years. Whether or not they would ever reach the gyre state is addressed in section 4.

Experiments 20 and 21 vary τ_0. In experiment 20, it is half of its normal value and the transport is about half that of experiment 15 (the control). It is still a β-plume after 100 years. In experiment 21, τ_0 is double its normal value, but the transport is 47 Sv, nearly six times that of experiment 15. (This data point is off the scale in Fig. 5.) However, experiment 15 is still a transient β-plume; the transport of a model that has attained a steady gyre circulation at the same $R_\beta(L/\delta_M)^2$ is about 22 Sv. The transport in experiment 21 is about twice this. In other words, the transport of both the gyre and β-plume branches increases roughly linearly with vorticity advection scale $R_\beta(L/\delta_M)^2$.

Table 1. Partial list of 8-level experiments to test the effect of variations in β, ν, and τ_0. See main text for definitions of all the parameters. Asterisks denote model times that started at the end of another experiment, not from rest.

Experiment	β $\times 10^{-11}$ $m^{-1}s^{-1}$	τ_0 Nm^{-2}	ν m^2s^{-1}	R_β $\times 10^{-3}$	Transport Sv	δ_I/L	δ_M/L	$R_\beta(L/\delta_M)^2$	Model time yr	Circulation type
β varying:										
1	1.22	−0.46	50	1.02	22.5	0.079	0.016	4.0	200	gyre
2	1.26	−0.46	50	0.96	21.6	0.078	0.016	3.8	200	gyre
3	1.30	−0.46	50	0.90	9.6	0.069	0.016	3.7	200	β-plume
4	1.35	−0.46	50	0.83	9.0	0.071	0.015	3.5	200	β-plume
5	1.40	−0.46	50	0.77	21.8	0.070	0.015	3.3	400	gyre
6	1.45	−0.46	50	0.72	21.3	0.068	0.015	3.2	400	gyre
7	1.50	−0.46	50	0.67	20.8	0.067	0.015	3.0	400	gyre
8	1.55	−0.46	50	0.63	20.4	0.066	0.015	2.9	400	gyre
9	2.00	−0.46	50	0.38	6.8	0.044	0.014	2.1	60*	β-plume
10	2.00	−0.46	50	0.38	17.4	0.058	0.014	2.1	10*	gyre
11	3.00	−0.46	50	0.17	5.2	0.041	0.012	1.2	110*	β-plume
12	3.00	−0.46	50	0.17	13.5	0.047	0.012	1.2	110*	gyre
13	4.00	−0.46	50	0.09	4.4	0.035	0.011	0.8	120*	β-plume
14	4.00	−0.46	50	0.09	9.2	0.040	0.011	0.8	110*	gyre
ν varying:										
15	1.29	−0.46	50	0.91	8.4	0.079	0.016	3.7	100	β-plume
16	1.29	−0.46	126	0.91	5.4	0.076	0.021	2.0	100	β-plume
17	1.29	−0.46	316	0.91	5.2	0.071	0.029	1.1	100	β-plume
18	1.29	−0.46	795	0.91	4.8	0.068	0.039	0.6	100	β-plume
19	1.29	−0.46	2,000	0.91	3.9	0.060	0.054	0.3	100	β-plume
τ_0 varying:										
20	1.29	−0.23	50	0.46	3.7	0.055	0.016	1.8	100	β-plume
21	1.29	−0.91	50	1.82	47.4	0.132	0.016	7.4	100	gyre

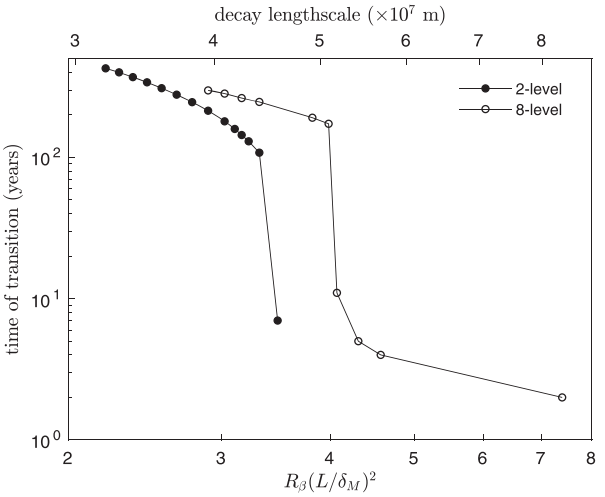

Figure 7. Time of transition from a β-plume to a gyre as a function of the characteristic scale of the vorticity advection term (lower x-axis, see Eq. 10) and the theoretical no-slip Munk decay length (upper x-axis, applies only to the 8-level data).

To summarize, strong enough forcing makes the flow more inertial (larger δ_I) and selects the gyre circulation. Conversely, increasing viscosity makes the flow less inertial and selects the β-plume circulation (experiments 15–19). These results are consistent with the idea that the β-plume solution applies if there is sufficient viscous interaction with the boundary to drain the imposed vorticity anomaly before the plume reaches back to the forcing region (see Section 4).

To study the time at which the circulation changes from a β-plume to a gyre, we select only those experiments that were run from start to finish with fixed parameters. Those that started at the end of another experiment with a different value of β are excluded. Of the selected experiments, the ones that showed a transition are plotted in Figure 7, with the vorticity advection scale Eq. (10) on the x-axis and the time of transition on the y-axis. Note that four 8-level simulations were run longer than 200 years, an exception to the cutoff time mentioned above. These are experiments 5–8 in Table 1.

Both the 2- and 8-level experiments show a jump in the time at which the transition occurs. For 2-levels, this happens at $R_\beta(L/\delta_M)^2 = 3.5$, and for 8-levels at 4.1. In both cases, the time of the transition increases by an order of magnitude, from $O(10)$ years to $O(100)$ years. Below these critical values, the time of the transition behaves as a power law with negative exponent, increasing apparently without bound as $R_\beta(L/\delta_M)^2 \to 0$. The upper limit of the data shows only the last known transition. 8-level experiments at $R_\beta(L/\delta_M)^2 < 2$, for example, likely also transition, but they evolve so slowly that it is unfeasible to run them long enough. The inverse relationship with the advection scale is not unexpected (a smaller

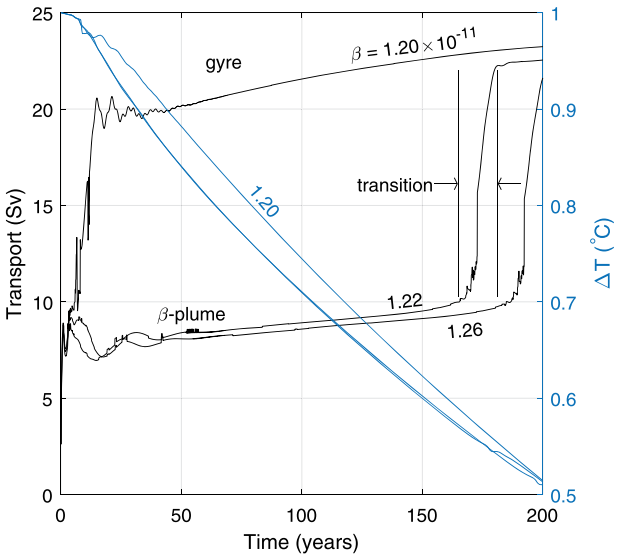

Figure 8. Transport in Sv (black) and temperature stratification ΔT (blue) as functions of time for three 8-level simulations. The corresponding values of β are given above the curves (in $\mathrm{m}^{-1}\mathrm{s}^{-1}$). The observed state of the circulation is labeled as a β-plume or a gyre, as well as the transition between them.

gradient in planetary vorticity or stronger wind forcing spins up the fluid faster), but the step change is. It is unclear why the time at which the transition occurs exhibits two regimes, and this is explored more below, but we speculate that it has to do with weak baroclinic effects in this nearly barotropic model.

We have performed similar simulations in a domain with no Greenland peninsula and obtained similar results. The models exhibit two types of circulation: a β-plume that extends westward, wrapping around the domain until it retroflects and returns to the forcing region, and a basin-wide gyre with stronger transport. The peninsula does not change the existence of these solutions, only their location in parameter space and the time at which the transition occurs. The important point is that the f/h contours are closed.

e. Stratification and slow adjustment

The vertical gradient in the temperature field is observed to decay exponentially with a timescale of 300 years. This loss of stratification imposes a similarly slow adjustment on the circulation. Figure 8 shows time series of transport (black) and ΔT (blue), where vertical temperature difference ΔT is taken at a point in the middle of the domain. The data are from three 8-level simulations with $\beta = 1.20$, 1.22, and 1.26×10^{-11} $\mathrm{m}^{-1}\mathrm{s}^{-1}$. Text annotations classify the transport as either β-plume (8–10 Sv) or gyre ($\gtrsim$ 20 Sv).

Figure 8 demonstrates several points: The two circulation modes, β-plume and gyre (identified above), clearly appear. The three simulations all begin as a β-plume and evolve into a gyre. The transition between modes is fast, with transport more than doubling in just 10 years. For $\beta = 1.22$ and 1.26×10^{-11} $m^{-1}s^{-1}$, the plume transport increases at a rate of 0.01 Sv/yr from 50 to 150 years. For $\beta = 1.20$, the gyre transport increases at a rate of 0.008 Sv/year at 200 years. By contrast, during the transition itself, the transport increases by 1 Sv/yr, namely one hundred times faster. We therefore refer to rates of $O(0.01)$ Sv/year as *nearly steady*. The time at which the transition occurs depends on β, and for $\beta = 1.20$–1.22×10^{-11} $m^{-1}s^{-1}$, it depends sensitively on β. A comprehensive explanation of this sensitivity is beyond the scope of this paper, but of great interest.

Figure 8 also shows that the exponential decay of ΔT with a timescale of about 300 years is essentially unaffected by the circulation (compare the three experiments). All simulations start at $\Delta T = 1°C$ and end at 0.5°C, despite very different circulation histories in between. However, the reverse does not seem to be true: the stratification affects the circulation. This decay superimposes a long timescale adjustment on the circulation. The circulation, and in particular the transition from β-plume to gyre, is sensitive to the stratification and hence its decay. The slow diffusion of temperature makes the flow more barotropic because it reduces baroclinic compensation. The flow is therefore more sensitive to the bottom bathymetry. The loss of stratification thereby strengthens the transport and favors the gyre circulation mode. The mechanism of this sensitivity is unclear, and the causal relationship between the changes in stratification and circulation deserves further study.

4. Vorticity budget

The results from section 3 suggest that the β-plume is not a stable solution in the current domain. The transition to a gyre occurs when the plume manages to encircle the basin and return to the forcing region. Thus, the downstream extent of the plume (measured counterclockwise from the forcing region) is the controlling factor. To quantify this extent, we would like to know the characteristic distance over which it decays.

HF16 showed that a β-plume with linear drag (the Stommel model) is compact in the presence of an obstructing western boundary. Friction balances the PV imparted by the wind and this causes the stream function to decay exponentially along the boundary. In comparison to the western boundary, friction at southern, eastern, and northern boundaries is negligible. The essential reason is that only at a western boundary do the f/h contours converge towards the wall (Fig. 2). These results were also shown to be true for a β-plume with horizontal viscosity (the Munk model). Viscous dissipation at the boundary balances the budget of PV and the stream function decays exponentially, though with a different *e*-folding length than the Stommel model. The data in HF16 Figure 8 are functions of θ, the angle of the obstructing boundary relative to west in an ocean with a flat seafloor, but the results are applicable to an ocean with varying bathymetry through the concept of dynamical west. We closely follow the derivation for the Stommel model

(given in HF16) to find dynamical west for the Munk model, which is the appropriate case here.

The Munk model is characterized by the steady, linear, barotropic vorticity equation with horizontal viscosity (HF16):

$$J\left(\psi, \frac{f}{h}\right) = \nu\nabla^2\left[\nabla\cdot\left(\frac{1}{h}\nabla\psi\right)\right] + \left(\frac{\partial F_y}{\partial x} - \frac{\partial F_x}{\partial y}\right). \tag{11}$$

Expanding and multiplying by h, we have

$$\begin{aligned}\psi_x\left[-\frac{fh_y}{h} + \frac{\nu}{h}\left(\frac{6h_xh_y^2}{h^2} - \frac{2h_xh_{yy}}{h} + \frac{6h_x^3}{h^2} - \frac{4h_yh_{xy}}{h} + h_{xyy} - \frac{6h_xh_{xx}}{h} + h_{xxx}\right) + \beta\right]\\ + \psi_y\left[+\frac{fh_x}{h} + \frac{\nu}{h}\left(\frac{6h_yh_x^2}{h^2} - \frac{2h_yh_{xx}}{h} + \frac{6h_y^3}{h^2} - \frac{4h_xh_{xy}}{h} + h_{xxy} - \frac{6h_yh_{yy}}{h} + h_{yyy}\right)\right]\\ = \nu\left(A\psi_{xx} + B\psi_{xy} + \cdots + \nabla^4\psi\right) + h\left(\frac{\partial F_y}{\partial x} - \frac{\partial F_x}{\partial y}\right),\end{aligned} \tag{12}$$

where A, B, ... are terms in h. The terms on the left-hand side can be rewritten as $\mathbf{u}\cdot\nabla\psi$, where the components of $\mathbf{u}$ (not the current associated with ψ; see below) are

$$u = \frac{fh_y}{h} - \frac{\nu}{h}\left(\frac{6h_xh_y^2}{h^2} - \frac{2h_xh_{yy}}{h} + \frac{6h_x^3}{h^2} - \frac{4h_yh_{xy}}{h} + h_{xyy} - \frac{6h_xh_{xx}}{h} + h_{xxx}\right) - \beta \tag{13}$$

and

$$v = -\frac{fh_x}{h} - \frac{\nu}{h}\left(\frac{6h_yh_x^2}{h^2} - \frac{2h_yh_{xx}}{h} + \frac{6h_y^3}{h^2} - \frac{4h_xh_{xy}}{h} + h_{xxy} - \frac{6h_yh_{yy}}{h} + h_{yyy}\right). \tag{14}$$

Eq. (11), then, can then be written as

$$\mathbf{u}\cdot\nabla\psi = \nu\left(A\psi_{xx} + B\psi_{xy} + \cdots + \nabla^4\psi\right) + Q, \tag{15}$$

which is analogous to an advection–diffusion equation in ψ with forcing Q. The stream function is "advected" in the direction defined by the pseudo-velocity vector $\mathbf{u}$. For constant layer thickness, i.e., $(u, v) = (-\beta, 0)$, ψ is distributed as if it is advected westwards at speed β. For a layer with varying thickness, the analogous advection components include bathymetric terms. These introduce a meridional component to the flow and distort $\mathbf{u}$ away from west. We refer to the resulting direction,

$$\theta_w = \tan^{-1}\left(\frac{v}{u}\right), \tag{16}$$

as dynamical west. It is the direction in which the stream function seems to be advected. The angle is measured positive counterclockwise from west and takes values in the interval $[-180°, 180°]$. The first terms in Eqs. (13) and (14) are proportional to f/h and advect ψ along h contours. Viscosity introduces many higher-order terms that are proportional to the partial derivatives of h. Strong gradients in layer thickness, large f, or large ν can all cause θ_w to point away from true west.

a. Idealized western boundary

Eqs. (13) and (14) are complex for a general thickness field, but we can simplify them by considering a western boundary with bathymetric variation only in x. Then they reduce to

$$u = -\frac{\nu}{h}\left(\frac{6h_x^3}{h^2} - \frac{6h_x h_{xx}}{h} + h_{xxx}\right) - \beta \tag{17}$$

$$v = -\frac{f h_x}{h}. \tag{18}$$

We let the western boundary slope exponentially with e-folding length l and abyssal depth H:

$$h(x) = H\left(1 - e^{-x/l}\right). \tag{19}$$

Plugging Eq. (19) into Eqs. (17) and (18) yields

$$u = -\frac{\nu}{l^3}\left(6\phi^3 + 6\phi^2 + \phi\right) - \beta \tag{20}$$

$$v = -\frac{f}{l}\phi, \tag{21}$$

where

$$\phi(x) = \frac{e^{-x/l}}{1 - e^{-x/l}}. \tag{22}$$

We are interested in the angle of intersection between dynamical west and the western boundary. We define a new angle

$$\theta = -\theta_w + 90°, \tag{23}$$

which is measured positive clockwise from south and also has a range $[-180°, 180°]$. When dynamical west is parallel to the western boundary, then the angle of intersection θ is zero. When dynamical west points into the boundary, then $\theta = 90°$, which is consistent with HF16.

Figure 9 is a contour plot with distance from the western boundary on the x-axis and β on the y-axis. The contours show $\log_{10}\theta$, where θ is measured in degrees. At all values of

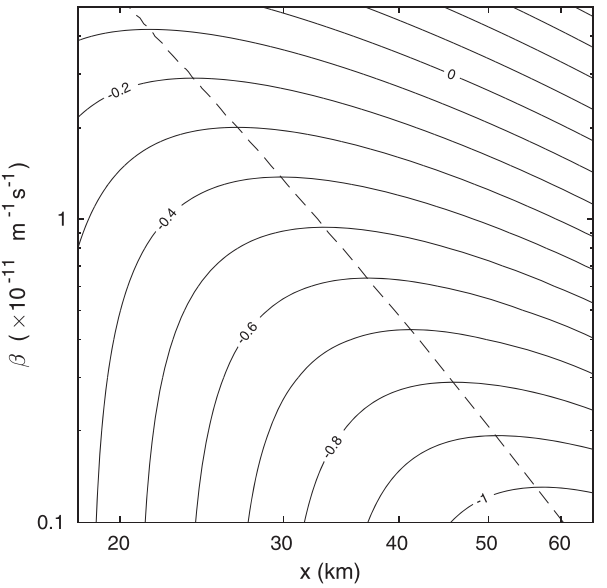

Figure 9. Contours of $\log_{10}\theta$, where θ is measured in degrees, as a function of distance from the western boundary and β. The dashed line traces out the minimum angle at every β.

β, there is a broad range near the boundary over which this angle is very small, less than 1°. The dashed line traces out the curve of minimum angles. Note that it is not at the boundary itself, but rather 20–30 km offshore. The minimum angle is of interest because it controls the maximum downstream distance reached by the plume (HF16). We expect that for a given β, water parcels offshore at the distance of the dashed line experience less dissipation than their neighbors and conserve more of their PV. They are the last to retroflect and therefore set the upper limit of the plume's extent.

Although θ is small along the western boundary in Figure 1b, it is a factor of 10–100 smaller along the southern boundary. This is because the high-order viscous terms in Eqs. (13) and (14) are very small. When they appear in the u term, as they do for a western boundary, β sets a lower limit on the magnitude of u and guarantees that $\mathbf{u}$ intersects the boundary. However, when they appear in the v term, as they would for a southern boundary, β does not appear and the magnitude of v is very small. Then $\mathbf{u}$ is nearly parallel to the boundary. θ is negative along the northern and eastern boundaries. Therefore nearly all of the dissipation happens along the western boundary and it is unnecessary to calculate θ anywhere else.

In HF16 the e-folding decay lengths of the β-plume tails for the Stommel and Munk models were calculated for wall intersection angles $3° < \theta < 50°$. Figure 10 shows $l_S = 2/(1 - \cos\theta)$, the theoretical decay length of the Stommel model (thin solid line). The data for the Munk model were determined numerically by solving the appropriate partial

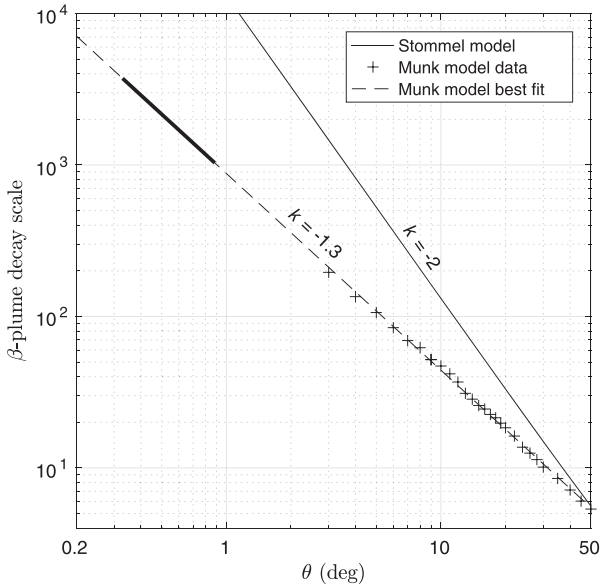

Figure 10. β-plume decay scales as a function of θ. Units are δ_S or δ_M. The thin solid line shows the theoretical asymptotic limit for the Stommel model, which is $2/(1-\cos\theta)$. The plus signs show the data from Haine and Fuller (2016) for the Munk β-plume with a no-slip boundary condition. The dashed line shows the best fit to the data and the thick line segment indicates the angles for which we need to know the decay scale. The equivalent power-law exponents are displayed next to the lines.

differential equation on a two-dimensional mesh with a narrow Gaussian forcing and a solid boundary. The results are shown by the plus signs. These scales have units of δ_S and δ_M, respectively, which in turn have units of meters. (Notice that δ_S and δ_M are usually associated with across-current scales; here, we use them to measure the along-current scale.) In this way we can compute $l_M\delta_M$, where l_M is the decay length of the Munk model (in units of δ_M) derived from the data in Figure 10. $l_M\delta_M$ therefore gives a decay scale for the Munk β-plume in meters, which can be compared to the length of the western boundary. If the western boundary is much longer than $l_M\delta_M$, there is sufficient distance to extract vorticity from the flow and we expect the plume to retroflect or at least noticeably weaken. If the western boundary is much shorter than $l_M\delta_M$, there is not sufficient distance and the plume should continue around the basin largely unaffected, ultimately reconnecting in the forcing region.

We extend the data for the Munk model to angles smaller than 3° by fitting a power law to them. The line of best fit is shown in Figure 10 (dashed line). The exponent of the power-law relationship is $k = -1.3$, which has a smaller absolute value than the exponent for the Stommel model, $k = -2$. This indicates that the decay scale in the Munk model

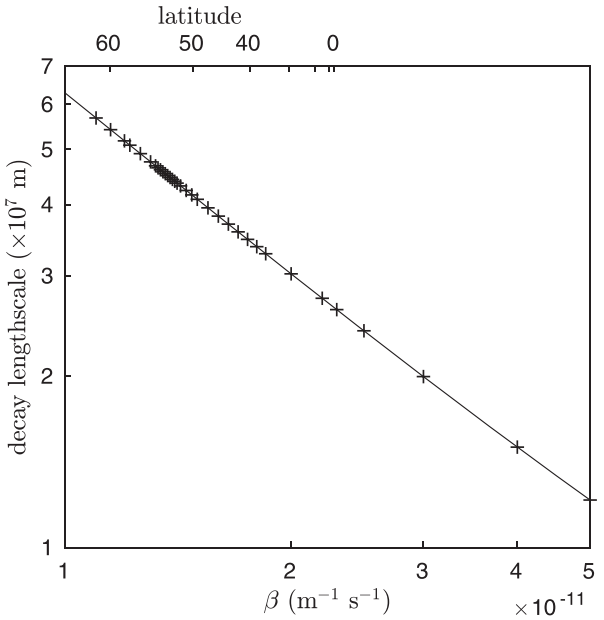

Figure 11. The Munk β-plume decay scale ($l_M \delta_M$) versus β for $\nu = 50$ m^{2}s^{-1}. The + symbols show the 8-level simulations from section 3 (Table 1). The upper x-axis shows the latitude corresponding to β, where it exists.

is a weaker function of the intersection angle than in the Stommel model, but still highly dependent on the angle. The thick line segment shows the range of angles that lie along the minimum curve in Figure 9 and for which we want to know l_M. Clearly at such small angles l_M is very large, $O(1{,}000\delta_M)$. Multiplying by δ_M produces the curve in Figure 11. β is plotted on the lower x-axis and the corresponding latitude, where it exists, is plotted on the upper x-axis. (On Earth, β does not exceed 2.3×10^{-11} m^{-1}s^{-1}.) The 8-level simulations from section 3 are indicated by + symbols. At small β, corresponding to small θ, the scale is $O(10^7)$ meters, which is many times longer than the western boundary (Fig. 1b). This falls off with increasing β, but for all values considered, $l_M \delta_M$ is 10 or more times the length of the western boundary in the model results shown above. This implies that for no value of β is a 900-km western boundary capable of extracting a large fraction of vorticity from the flow.

This explains the results of section 3, where we conjectured that every model, given enough time, eventually reaches a gyre state. As the models spin up and a β-plume forms, it slowly but continuously spreads around the domain, following contours of f/h. Once the SSH lines reenter the forcing region, the wind is able to spin up the water repeatedly and the circulation proceeds quickly to a gyre.

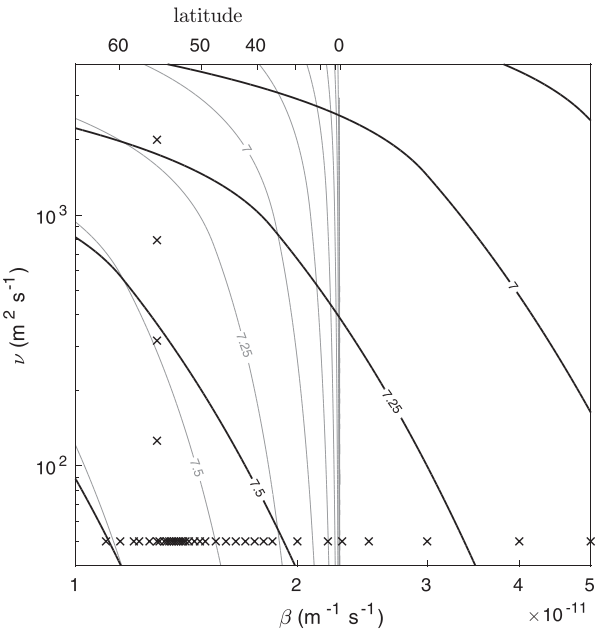

Figure 12. Contours of $\log_{10}(l_M \delta_M)$, where $l_M \delta_M$ is measured in meters, plotted as a function of β and horizontal viscosity ν. The thick black contours show l_M calculated using the β-plane approximation; the thin gray contours show l_M calculated using spherical coordinates. All models were run on a β-plane. The × symbols show the 8-level experiments from section 3 (Table 1; Fig. 11). The upper x-axis shows the latitude corresponding to β, where it exists.

We can use the data in Figure 11 to revisit the time of the transition in Figure 7 and instead plot it against the theoretical decay length. This is shown along the upper x-axis in Figure 7, which applies only to the 8-level data. The jump is at 5.1×10^7 m, which is not an obviously special length. It is about 60 times the length of the western boundary or 12 times the circumference of the domain. It remains unclear why the time of the transition is so sensitive at this particular decay length or value of $R_\beta (L/\delta_M)^2$.

So far we have used $\nu = 50$ m^{2}s^{-1}. How does the decay scale $l_M \delta_M$ change for other values? Intuitively, we expect that as the flow becomes more viscous, the β-plume has a shorter decay scale. This is evident from Eq. (3), which suggests a weak dependence on ν. But the decay scale also changes through the angle of dynamical west (Eq. 16), which determines l_M.

Figure 12 shows a contour plot of $\log_{10}(l_M \delta_M)$ in the space of β and ν. The thick black contours were calculated using the β-plane approximation. The thin gray contours were calculated using spherical coordinates. The equivalent latitude is shown on the upper x-axis, where it exists. All simulations were run on a β-plane; the spherical coordinate contours are shown only for reference. The 8-level simulations are indicated by × symbols.

The model western boundary is 900 km $= 10^{5.95}$ m. Therefore we do not expect noticeable dissipation to occur unless the choices of β and ν place $l_M \delta_M$ above and to the right of the 6 contour. However, this contour does not appear in Figure 12 for the β-plane approximation, and it appears only very near the equator in spherical coordinates. In other words, under this theory, a mid-latitude β-plume is an impossible steady state given the dimensions of the domain, $\beta < 5 \times 10^{-11}$ m^{-1}s^{-1}, and $40 < \nu < 4{,}000$ m^{2}s^{-1}. Only with wildly unrealistic parameter choices could we force $l_M \delta_M$ to approach 900 km. Over most of Figure 12, it is an order of magnitude or more larger than 900 km.

Is a steady β-plume simply impossible then? Restricting ourselves to reasonable choices for β, ν, and the length of the western boundary, the only remaining parameter is l, the decay scale of the bathymetry at the sidewall. This controls $l_M \delta_M$ in a complex way that we cannot explore here, but it may be possible that a low-latitude basin with steep sidewalls and high eddy viscosity could permit a steady β-plume.

b. The Labrador Sea

We now apply the same arguments to the bathymetry of the Labrador Sea. High-resolution data is obtained from the British Oceanographic Data Centre (IOC et al. 2003) and smoothed using a two-dimensional Gaussian filter with a standard deviation of 2 km. Where the direction of dynamical west points into the seafloor, the decay length of the no-slip Munk β-plume is calculated using the best-fit power-law relationship and then scaled by the local value of δ_M, with $\nu = 500$ m^{2}s^{-1} (Funk et al. 2009). The result is shown in Figure 13. White indicates areas where the local direction of dynamical west points away from the seafloor, and so the theory of HF16 does not apply, or the dynamical west vector is trivially short. The color bar stops at 10,000 km. The western continental shelf of the Labrador Sea has decay lengths of several thousands of kilometers, with some areas exceeding 10,000 km. Because this is clearly larger than the scale of the Labrador Sea, it implies that a steady, linear, barotropic circulation with Laplacian viscosity would be mostly undamped in its transit around the continental shelf. The circulation would not be expected to retroflect. The shortest decay lengths appear around Greenland. These are $O(1{,}000)$ km or less in places. This is still comparable to the length of the southern Greenland coast, but does admit the possibility of strong damping of the boundary current. Compare this with the mid-depth stream function in Faure and Speer (2005), Figure 6a. The boundary current circumnavigating the Labrador Sea does not show any retroflections, in agreement with the decay length theory. Both figures, however, assume barotropicity from the start, which is not strictly accurate.

5. Discussion and conclusions

We use MITgcm to investigate the nature of wind-forced circulations in an idealized model of the subpolar North Atlantic with closed f/h contours. The forcing is designed to exert cyclonic wind stress curl over a small region of the basin, similar to the point source

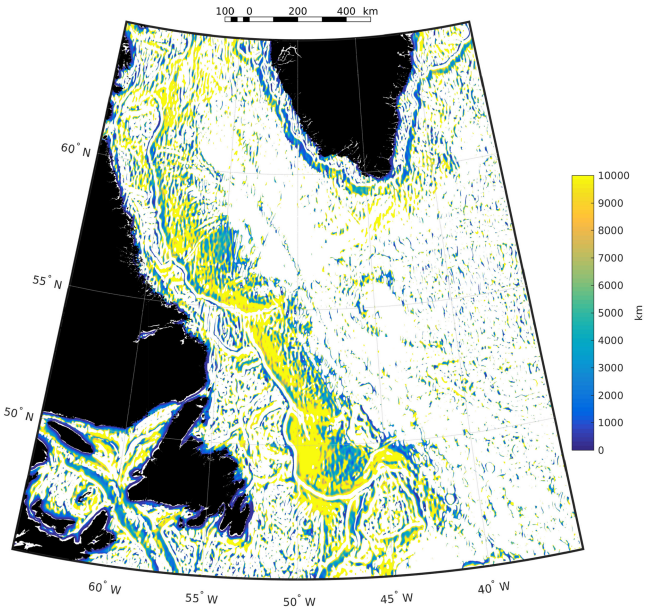

Figure 13. Decay length (in km) of the no-slip Munk β-plume in the Labrador Sea. Bathymetry data is taken from the British Oceanographic Data Centre (IOC et al. 2003) and smoothed with a Gaussian filter.

vorticity forcing in HF16. The initial response of the ocean is a bathymetric β-plume, i.e., a β-plume that is steered mainly by changes in layer thickness, not by changes in the Coriolis parameter. The wind drives a westward flow around Greenland and south along the western boundary. The current then retroflects and returns to the forcing region, closing the circulation.

In the long-term, however, the β-plume evolves counterclockwise around the basin until it reenters the forcing region from the east. At this point, a rapid transition to a basin-wide gyre occurs. This transition occurs over a wide range of β, wind forcing, and viscosity, although the time at which the transition occurs is sensitive to these parameters. In simulations with eight vertical levels, the gyre solution seems to persist indefinitely. In simulations with two levels, for large β, the β-plume persists as a quasi-steady state: after several hundred years of model time, the β-plume has not yet transitioned to a gyre, but we cannot say that it is unconditionally steady. The transport of the gyre is two to three times higher than the transport of the β-plume. It is unclear what controls the timing of the rapid transition, but weak baroclinic effects seem to be important.

Assuming linear barotropic theory, an analysis of the budget of PV along the western boundary suggests an explanation for the ultimate preference for a gyre circulation rather than a β-plume. This follows the work of HF16, who analyzed the PV budget of a coastal

β-plume forced by a point source. For all realistic choices of parameters, the western boundary of the idealized model is much shorter than the predicted decay scale of the β-plume. This means that there is not enough distance along the western boundary for dissipation to drain the vorticity imparted by the wind. Therefore the β-plume continues to encircle the domain, and the observed trend towards a basin-filling gyre seems inevitable. However, the float data clearly show that there are permanent recirculating cells in the Labrador Sea. What explains this disagreement?

At least one of the assumptions underlying the theory of HF16 must be broken. They assumed that the flow is steady, linear (relative vorticity is much less than the background planetary vorticity), barotropic, forced by a point source of vorticity, and bounded by a straight wall. Although none of these is strictly true in the Labrador Sea, we suspect it is the assumption of linearity that breaks down in places where the bathymetry is steep and/or turns sharply. The answer therefore may be that β-plumes form under regions of localized vorticity forcing and expand to fill smooth stretches of the shelf break, but the flow becomes nonlinear at sharp bathymetric features, such as Eirik Ridge, Hamilton Bank, and Flemish Cap (see Fig. 1). There, inertial separation causes the flow to deviate from f/h contours and relative vorticity becomes important. Because viscous dissipation acts most strongly where relative vorticity is concentrated ($\nu\nabla^2\zeta$), the flow loses vorticity at these points and retroflects. In this view, the western boundary of the Labrador Sea is not long enough to support a recirculating β-plume, as suggested by Figure 13, but they exist nonetheless because sharp bathymetric gradients break the Lagrangian conservation of planetary PV. According to this idea, recirculations in the subpolar North Atlantic are best understood as inherently unsteady features that are maintained by the local bathymetry. Specifically, in a domain with realistic horizontal extent and bathymetric slope, recirculations driven by strong forcing are only quasi-steady because frictional dissipation of vorticity is not generally strong enough to balance the input of vorticity from the wind.

So far we have ignored the effects of mixing between water masses, but this is an important effect in the Labrador Sea. Near Flemish Cap and the Grand Banks, southward flowing LSW encounters the northward flowing North Atlantic Current. The majority of LSW at 50°N leaves the continental slope and entrains in the ocean interior (Bower et al. 2011). Only a small fraction flows continuously south. In addition to sharp bathymetric gradients, interaction with the counter-flowing western boundary current may also explain why β-plumes are observed despite the long decay scales of the Labrador Sea.

In addition, baroclinic effects may be important, although they are weak overall in our model. Baroclinic effects can drive steady, linear, depth-averaged flow across f/h contours over sloping bathymetry. This baroclinic compensation decouples the near-surface flow from bathymetric vorticity constraints. The stratification shields the depth-averaged flow, and hence the surface flow, from strong gradients in f/h at the edges of the domain. This reduces the apparent magnitude of ∇h and makes dynamical west point more in the direction of true west. At a western boundary, this means a larger intersection angle, which, according to Figure 10, corresponds to a shorter decay scale and therefore favors a β-plume

solution. Indeed, as the stratification slowly erodes by diffusion, the baroclinic compensation diminishes and the circulation switches to the gyre mode that follows f/h contours.

The opportunity for nonlinearity to distort PV through the layer thickness, in addition to the relative vorticity, presumably also introduces new phenomena in a nonlinear baroclinic model. Future work should explore these effects more, focusing on the slow evolution of the β-plume. Additionally, recall that R_β is proportional to τ_0/β^2. Changes in τ_0 affect R_β, but changes in β affect both R_β and the distribution of f/h contours. Therefore τ_0 is a more precise way to control R_β without simultaneously altering the f/h field. Varying β conflates the two effects. Future work should therefore span a range of R_β by varying τ_0 and leaving β fixed. Only two such experiments (20 and 21) were carried out in this study.

Acknowledgments. AMF was supported by the National Science Foundation IGERT Program in Modeling Complex Systems. Discussion with Michael Spall helped clarify the paper.

REFERENCES

Bogden, P. S., R. E. Davis, and R. Salmon. 1993. The North Atlantic circulation: combining simplified dynamics with hydrographic data. J. Mar. Res., *51*, 1–52. doi: 10.1357/0022240933223855

Bower, A., S. Lozier, and S. Gary. 2011. Export of Labrador Sea Water from the subpolar North Atlantic: a Lagrangian perspective. Deep-Sea Res. II, *58* (17), 1798–1818. doi: 10.1016/j.dsr2.2010.10.060

Daniault, N., P. Lherminier, and H. Mercier. 2011. Circulation and transport at the southeast tip of Greenland. J. Phys. Oceanogr., *41*, 437–457. doi: 10.1175/2010JPO4428.1

Deshayes, J., C. Frankignoul, and H. Drange. 2007. Formation and export of deep water in the Labrador and Irminger Seas in a GCM. Deep-Sea Res. I, *54*, 510–532. doi: 10.1016/j.dsr.2006.12.014

Faure, V., and K. Speer. 2005. Labrador Sea Water circulation in the northern North Atlantic Ocean. Deep-Sea Res. II, *52*, 565–581. doi: 10.1016/j.dsr2.2004.12.004

Forget, G., H. Mercier, and B. Ferron. 2008. Combining Argo profiles with a general circulation model in the North Atlantic. Part 2: realistic transports and improved hydrography, between spring 2002 and spring 2003. Ocean Model., *20*, 17–34. doi: 10.1016/j.ocemod.2007.06.002

Funk, A., P. Brandt, and T. Fischer. 2009. Eddy diffusivities estimated from observations in the Labrador Sea. J. Geophys. Res., *114*, C04001. doi: 10.1029/2008JC005098

Haine, T., C. Böning, P. Brandt, J. Fischer, A. Funk, D. Kieke, et al. 2008. North Atlantic Deep Water formation in the Labrador Sea, recirculation through the subpolar gyre, and discharge to the subtropics, *in* Arctic-Subarctic Ocean Fluxes: Defining the role of the Northern Seas in Climate, R. R. Dickson, J. Meincke, and P. Rhines, eds. Berlin: Springer Verlag, 653–701. doi: 10.1007/978-1-4020-6774-7_28

Haine, T., and A. Fuller. 2016. Boundary β-plumes and their vorticity budgets. Q. J. Roy. Meteor. Soc., *142*, 2758–2767. doi: 10.1002/qj.2866

Hall, M. M., D. J. Torres, and I. Yashayaev. 2013. Absolute velocity along the AR7W section in the Labrador Sea. Deep-Sea Res. I, *72*, 72–87. doi: 10.1016/j.dsr.2012.11.005

Holliday, N. P., A. Meyer, S. Bacon, S. G. Alderson, and B. de Cuevas. 2007. Retroflection of part of the east Greenland current at Cape Farewell. Geophys. Res. Lett., *34*, L07609. doi: 10.1029/2006GL029085

Holliday, N., S. Bacon, J. Allen, and E. McDonagh. 2009. Circulation and transport in the western boundary currents at Cape Farewell, Greenland. J. Phys. Oceanogr., *39*, 1854–1870. doi: 10.1175/2009JPO4160.1

IOC, IHO (International Hydrographic Organization), and BODC (British Oceanographic Data Centre). 2003. Centenary edition of the GEBCO digital atlas. Technical report, British Oceanographic Data Centre, Liverpool.

Käse, R. H., A. Biastoch, and D. B. Stammer. 2001. On the mid-depth circulation in the Labrador and Irminger Seas. Geophys. Res. Lett., *28*, 3433–3436. doi: 10.1029/2001GL013192

Koblinsky, C. J. 1990. The global distribution of f/H and the barotropic response of the ocean. J. Geophys. Res., *95*, 3213–321. doi: 10.1029/JC095iC03p03213

Lavender, K. L., W. Brechner Owens, and R. E. Davis. 2005. The mid-depth circulation of the subpolar North Atlantic Ocean as measured by subsurface floats. Deep-Sea Res. I, *52*, 767–785. doi: 10.1016/j.dsr.2004.12.007

Lavender, K. L., R. E. Davis, and W. Brechner Owens. 2000. Mid-depth recirculation observed in the interior Labrador and Irminger seas by direct velocity measurements. Nature, *407*, 66–69. doi: 10.1038/35024048

Lilly, J. M., P. B. Rhines, F. Schott, K. L. Lavender, J. Lazier, U. Send, and E. D'Asaro. 2003. Observations of the Labrador Sea eddy field. Prog. Oceanogr., *59*, 75–176. doi: 10.1016/j.pocean.2003.08.013

Marshall, D. 1995. Influence of topography on the large-scale ocean circulation. J. Phys. Oceanogr., *25*, 1622–1635. doi: 10.1175/1520-0485(1995)025<1622:IOTOTL>2.0.CO;2

Marshall, J., A. Adcroft, C. Hill, L. Perelman, and C. Heisey. 1997. A finite-volume, incompressible Navier Stokes model for studies of the ocean on parallel computers. J. Geophys. Res. Oceans, *102*, 5753–5766. doi: 10.1029/96JC02775

Marshall, D. P., and J. C. Stephens. 2001. On the insensitivity of the wind-driven circulation to bottom topography. J. Mar. Res., *59*, 1–27. doi: 10.1357/002224001321237344

Mesinger, F., G. DiMego, E. Kalnay, K. Mitchell, P. C. Shafran, W. Ebisuzaki, et al. 2006. North American regional reanalysis. Bull. Am. Meteorol. Soc., *87*, 343–360. doi: 10.1175/BAMS-87-3-343

Munk, W. H. 1950. On the wind-driven ocean circulation. J. Meteorol., *7* (2), 80–93.

Palter, J. B., M. S. Lozier, and K. L. Lavender. 2008. How does Labrador Sea Water enter the deep western boundary current? J. Phys. Oceanogr., *38*, 968–983. doi: 10.1175/2007JPO3807.1

Pedlosky, J. 1987. Geophysical Fluid Dynamics. New York: Springer-Verlag.

Pedlosky, J. 1996. Ocean Circulation Theory. New York: Springer-Verlag.

Pickart, R. S., M. A. Spall, M. H. Ribergaard, G. W. K. Moore, and R. F. Milliff. 2003. Deep convection in the Irminger Sea forced by the Greenland tip jet. Nature, *424*, 152–156. doi: 10.1038/nature01729

Renfrew, I. A., G. W. K. Moore, P. S. Guest, and K. Bumke. 2002. A comparison of surface layer and surface turbulent flux observations over the Labrador Sea with ECMWF analyses and NCEP reanalyses. J. Phys. Oceanogr., *32*, 383–400. doi: 10.1175/1520-0485(2002)032<0383:ACOSLA>2.0.CO;2

Schmitz, W. J., and M. S. McCartney. 1993. On the North Atlantic circulation. Rev. Geophys., *31*, 29–49. doi: 10.1029/92RG02583

Spall, M. A. 1996. Dynamics of the Gulf Stream/Deep Western Boundary Current crossover. Part I: entrainment and recirculation. J. Phys. Oceanogr., *26* (10), 2152–2168. doi: 10.1175/1520-0485(1996)026<2152:DOTGSW>2.0.CO;2

Spall, M. A., and R. S. Pickart. 2003. Wind-driven recirculations and exchange in the Labrador and Irminger Seas. J. Phys. Oceanogr., *33*, 1829–1845. doi: 10.1175/2384.1

Stommel, H. 1982. Is the South Pacific helium-3 plume dynamically active? Earth Planet. Sci. Lett., *61*, 63–67. doi: 10.1016/0012-821X(82)90038-3

Sverdrup, H. U., M. W. Johnson, and R. H. Fleming. 1942. The Oceans, Their Physics, Chemistry, and General Biology. New York: Prentice-Hall.

Våge, K., R. S. Pickart, A. Sarafanov, Ø. Knutsen, H. Mercier, P. Lherminier, et al. 2011. The Irminger Gyre: circulation, convection, and interannual variability. Deep-Sea Res. I, *58*, 590–614. doi: 10.1016/j.dsr.2011.03.001

Vallis, G. K. 2006. Atmospheric and Oceanic Fluid Dynamics: Fundamentals and Large-Scale Circulation. New York: Cambridge University Press.

Received: *17 July 2017*; revised: *24 April 2019*.